

Squeezing via self-induced transparency in mercury-filled photonic crystal fibers

M. S. NAJAFABADI,^{1,*} J. F. CORNEY,² L. L. SÁNCHEZ-SOTO,^{1,3} N. Y. JOLY,^{5,1} AND G. LEUCHS^{1,5}

¹Max-Planck-Institut für die Physik des Lichts, 91058 Erlangen, Germany

²School of Mathematics and Physics, University of Queensland, Brisbane, Queensland 4072, Australia

³Departamento de Óptica, Facultad de Física, Universidad Complutense, 28040 Madrid, Spain

⁵Institut für Optik, Information und Photonik, Friedrich-Alexander-Universität Erlangen-Nürnberg, 91058 Erlangen, Germany

*mojdeh.shikhali-najafabadi@mpl.mpg.de

Abstract: We investigate the squeezing of ultrashort pulses using self-induced transparency in a mercury-filled hollow-core photonic crystal fiber. Our focus is on quadrature squeezing at low mercury vapor pressures, with atoms near resonance on the $^3D_3 \rightarrow 6^3P_2$ transition. We vary the atomic density, thus the gas pressure (from 2.72 to 15.7 μbar), by adjusting the temperature (from 273 K to 303 K). Our results show that achieving squeezing at room temperature, considering both fermionic and bosonic mercury isotopes, requires ultrashort femtosecond pulses. We also determine the optimal detection length for squeezing at different pressures and temperatures.

1. Introduction

Self-induced transparency (SIT) is a well-established phenomenon in nonlinear optics, where a coherent light pulse can propagate through a resonant medium without being absorbed, even though the medium would typically be opaque at that frequency. This effect was first reported by McCall and Hahn [1, 2], who, using a semiclassical approach, showed that a two-level medium becomes transparent to a pulse with an area of 2π . Since then, SIT has been observed across various media (for comprehensive reviews, see [3–6]).

While there are several popular methods for generating squeezed states, these processes often have limitations, such as high-power requirements and phase-matching sensitivity, which complicate their application. SIT offers a unique alternative by leveraging coherent atomic population oscillations, which do not require strong pump fields, reducing the need for high-intensity lasers. Additionally, SIT avoids strict phase-matching conditions, making it easier to implement. Thus, SIT solitons have emerged as promising candidates for generating squeezed states, overcoming many challenges posed by traditional methods [7].

However, experimental demonstrations in gases have remained elusive. To overcome these challenges, gas-filled hollow-core photonic crystal fibers (PCFs) have emerged as an alternative for squeezing generation. These fibers exploit the strong nonlinearity of atomic transitions alongside a tight transverse confinement of light [8, 9]. A notable advantage of this approach is the ability to fine-tune the nonlinearity by adjusting the gas pressure.

Despite their potential, gas-filled PCFs also pose certain challenges, particularly in filling them with a suitable gas [10]. For instance, alkali vapors, such as rubidium, tend to bond with and diffuse into the glass walls, complicating the process of maintaining a consistent pressure [11]. Recent advancements, however, have demonstrated that it is possible to neatly fill hollow-core PCFs with rubidium in an adapted setup [12].

Alternatively, mercury has been suggested as a filling gas [13], owing to its high vapor pressure at room temperature, which prevents condensation on the glass. Moreover, mercury demonstrates significant optical nonlinearities in the ultraviolet and blue regions of the spectrum.

In this paper, we conduct a comprehensive investigation into the feasibility of utilizing mercury-filled PCFs for the generation of pulsed squeezed states. To achieve this, we adapt a method

for studying the propagation of radiation within an optically pumped two-level system, incorporating both collisional and radiative damping effects [14]. The approach involves deriving a set of stochastic c -number differential equations that are equivalent to the Heisenberg operator equations. This is done using the positive- P representation [15], which provides a probabilistic framework wherein stochastic averages correspond to normally ordered correlations. A significant advantage of this technique is its ability to yield numerically solvable equations while retaining key aspects that represent the quantum nature of the field.

The structure of this paper is as follows: In Sec 2, we introduce the model Hamiltonian and investigate how quantum noise sources arise from both damping and nonlinearities. We explore the dynamics by numerically solving the fully nonlinear stochastic differential equations derived from the positive P representation, building upon our previous work [16]. In Sec 4, we present the main results of our model. First, we demonstrate that when considering only the isotope ^{202}Hg in the sample, the squeezing is several dB higher than in a sample containing all isotopes at 273 K. Additionally, we examine the effect of detuning on squeezing for ^{202}Hg at 273 and 293 K, showing how detuning improves squeezing at these temperatures. Finally, we derive the optimal squeezing for a range of temperatures and determine the corresponding detection lengths for each case. Finally, our conclusions are summarized in Sec 5.

2. Model Hamiltonian

To make this paper as self-contained as possible, we will briefly review the model we use. Based on the ideas in Ref. [14], we present a Hamiltonian that describes the interaction between an ensemble of two-level atoms and a single mode of the radiation field. In the rotating-wave and dipole approximations, this Hamiltonian reads

$$\hat{H} = \hat{H}_A + \hat{H}_F + \hat{H}_B + \hat{H}_{FB} + \hat{H}_{AB} + \hat{H}_{AF} \quad (1)$$

where

$$\begin{aligned} \hat{H}_A &= \frac{1}{2} \sum_{\mu} \hbar \omega_{\mu} \hat{\sigma}_{\mu}^3, \\ \hat{H}_F &= \sum_k \hbar \omega_k \hat{a}_k^{\dagger} \hat{a}_k, \\ \hat{H}_B &= \hat{H}^a + \hat{H}^{\sigma} + \hat{H}^z, \\ \hat{H}_{AF} &= \hbar \sum_k \sum_{\mu} (g \hat{a}_k^{\dagger} \hat{\sigma}_{\mu}^{-} e^{-ikz_{\mu}} + \text{H.c.}), \end{aligned} \quad (2)$$

In this model, \hat{H}_A represents the free Hamiltonian of the atoms, where ω_{μ} is the resonant frequency of the μ th atom, described using standard Pauli operators [17]. Similarly, \hat{H}_F represents the free Hamiltonian of the field modes traveling through the fiber, with each mode characterized by a frequency ω_k and annihilation operator \hat{a}_k (for a single polarization).

The term \hat{H}_B is the free Hamiltonian of the reservoirs, which includes contributions from the field modes (\hat{H}^a), atomic dipoles (\hat{H}^{σ}), and collisions (\hat{H}^z). The interaction between the field and atomic dipoles is described by \hat{H}_{AF} , with a dipole-field coupling constant g , assumed to be the same for all atoms and independent of frequency and wave vector. The Hamiltonian \hat{H}_{AB} accounts for the interaction between the atomic reservoirs and atoms, while \hat{H}_{FB} describes the interaction of the background reservoir with the radiation field.

The system's evolution can be studied through the master equation. By tracing out the reservoir variables and applying the standard Markov approximation [17], we obtain:

$$\frac{d\hat{\rho}}{dt} = \frac{1}{i\hbar} [\hat{H}, \hat{\rho}] + \hat{\mathcal{L}}_{AB}[\hat{\rho}] + \hat{\mathcal{L}}_{FB}[\hat{\rho}], \quad (3)$$

where $\hat{\rho}$ is the density matrix of the system. The Lindblad superoperators $\hat{\mathcal{L}}_{\text{AB}}$ and $\hat{\mathcal{L}}_{\text{FB}}$ describe relaxation processes in the atomic and field variables, respectively, taking the following form:

$$\begin{aligned}\hat{\mathcal{L}}_{\text{AB}}[\hat{\rho}] &= \sum_{\mu} \frac{1}{2} W_{21}([\hat{\sigma}_{\mu}^{-} \hat{\rho}, \hat{\sigma}_{\mu}^{+}] + [\hat{\sigma}_{\mu}^{-}, \hat{\rho} \hat{\sigma}_{\mu}^{+}]) + \frac{1}{2} W_{12}([\sigma_{\mu}^{+} \hat{\rho}, \hat{\sigma}_{\mu}^{-}] + [\sigma_{\mu}^{+}, \hat{\rho} \hat{\sigma}_{\mu}^{-}]) + \frac{1}{4} \gamma_p([\hat{\sigma}_{\mu}^3, \hat{\rho} \hat{\sigma}_{\mu}^3] + [\hat{\sigma}_{\mu}^3, \hat{\rho} \hat{\sigma}_{\mu}^3]), \\ \hat{\mathcal{L}}_{\text{FB}}[\hat{\rho}] &= \frac{1}{2} c \kappa \sum_k (1 + \bar{n})([\hat{a}_k \hat{\rho}, \hat{a}_k^{\dagger}] + [\hat{a}_k, \hat{\rho} \hat{a}_k^{\dagger}]) + \bar{n}([\hat{a}_k^{\dagger} \hat{\rho}, \hat{a}_k] + [\hat{a}_k^{\dagger}, \hat{\rho} \hat{a}_k]).\end{aligned}\tag{4}$$

Here, W_{21} is the relaxation rate from the excited to the ground state, W_{12} is the incoherent pumping rate, and $\gamma_p = 3\gamma_0$ is the pure dephasing rate. For the field, κ is the absorption rate during the propagation within the medium and

$$\bar{n} = \frac{1}{\exp\left(\frac{\hbar\omega_p}{k_B T_f}\right) - 1}\tag{5}$$

is the mean equilibrium photon number in each reservoir mode of interest with T_f to be temperature of the field background reservoir. If we consider the thermal temperature of the radiative reservoir for the atoms to be T_a , then:

$$W_{21} = \gamma_0(1 + \bar{n}_a), \quad W_{12} = \gamma_0 \bar{n}_a,\tag{6}$$

with photon occupation number \bar{n}_a given by (5) with temperature T_a .

The damping rates are

$$\gamma_{\parallel} = W_{12} + W_{21}, \quad \gamma_{\perp} = \gamma_p + \frac{1}{2}\gamma_{\parallel}.\tag{7}$$

These coefficients γ_{\parallel} and γ_{\perp} correspond to two different damping mechanisms; namely, longitudinal (population decay) and transverse (dephasing).

We assume that only one transverse mode of the optical waveguide is relevant, meaning that other transverse modes are either unsupported by the waveguide or not excited during propagation. Additionally, the transverse mode profile $u(\mathbf{r}_{\perp})$ remains uniform along the length of the fiber. The relevant electromagnetic modes are those with wave vectors aligned along the waveguide axis (assumed to be the z axis). Therefore, we can define the optical field (scaled to the Rabi frequency) at position z_l as

$$\hat{\Omega}(z_l) \equiv 2ig \sum_m e^{ik_m z_l} \hat{a}_m.\tag{8}$$

Here, \hat{a}_m are the annihilation operators for modes with frequency ω_m and corresponding wavenumbers $k_m = m\Delta k$, where $\Delta k = 2\pi/L$ and L is the quantization length (i.e., length of fibre).

We define the atomic field operators by adding together the operators for individual atoms in a given spatial cell at \mathbf{r}_j and within the frequency band centred at ω_m :

$$\begin{aligned}\hat{R}^3(\mathbf{r}_j, \omega_m) &\equiv \frac{1}{N_{jm}} \sum_n^{N_{jm}} \hat{\sigma}_{jmn}^3, \\ \hat{R}^{\pm}(\mathbf{r}_j, \omega_m) &\equiv \frac{2}{N_{jm}} \sum_n^{N_{jm}} \hat{\sigma}_{jmn}^{\pm};\end{aligned}\tag{9}$$

where the atomic index $\mu = (j, m, n)$ has been expanded so that we can sum over only those atoms satisfying the above conditions. Note that the number of atoms in each spatio-frequency

cell can be written as $N_{jm} = \rho(\mathbf{r}_j, \omega_m) \Delta V \Delta \omega$, where $\rho(\mathbf{r}_j, \omega_m)$ is the density of resonant atoms in \mathbf{r}_j and a certain frequency ω_m .

Using standard methods one can derive the corresponding master equation. However, its direct numerical integration is extremely difficult. For that reason, our strategy is to derive suitable equations of motion in phase space. We use the positive P approach [15], which is a normally ordered operator representation that identifies the moments of $\hat{\rho}$ with the corresponding c -number moments of a positive P distribution.

In this approach, we have a mapping $\hat{\Omega} \leftrightarrow \Omega$, $\hat{\Omega}^\dagger \leftrightarrow \Omega^\dagger$, $\hat{R}^\pm \leftrightarrow R^\pm$, $\hat{R}^3 \leftrightarrow R^3$ and, following the standard procedures, the master equation can then be transformed into an equivalent Fokker-Planck equation for $P(\Omega, \Omega^\dagger, R^-, R^+, R^3)$. This equation is valid only when the distribution $P(\Omega, \Omega^\dagger, R^-, R^+, R^3)$ vanishes sufficiently rapidly at the boundaries. In practical applications, it is usually the case that the damping terms provide a strong bound at infinity on the distribution function [18].

In terms of these variables, and in the limit of large number of atoms, we get the following set of stochastic equations that serve as the basis for the simulation:

$$\begin{aligned} \left(\frac{\partial}{\partial z} + \frac{1}{c} \frac{\partial}{\partial t} \right) \Omega(t, z) &= -\frac{1}{2} \kappa \Omega(t, z) + G \int \rho(\mathbf{r}, \omega) R^-(t, \mathbf{r}, \omega) d\mathbf{r}_\perp d\omega + F^\Omega(t, z), \\ \frac{\partial}{\partial t} R^-(t, \mathbf{r}, \omega) &= -[\gamma_\perp + i(\omega - \omega_0)] R^-(t, \mathbf{r}, \omega) + u(\mathbf{r}_\perp) \Omega(t, z) R^3(t, \mathbf{r}, \omega) + F^R(t, \mathbf{r}, \omega), \\ \frac{\partial}{\partial t} R^3(t, \mathbf{r}, \omega) &= -\gamma_\parallel [R^3(t, \mathbf{r}, \omega) - \sigma^{SS}] - \frac{1}{2} [u(\mathbf{r}_\perp) \Omega(t, z) R^+(t, \mathbf{r}, \omega) + u^*(\mathbf{r}_\perp) \Omega^\dagger(t, z) R^-(t, \mathbf{r}, \omega)] + F^z(t, \mathbf{r}, \omega), \end{aligned} \quad (10)$$

where

$$\sigma^{SS} = \frac{W_{12} - W_{21}}{W_{12} + W_{21}}, \quad G = \frac{Lg^2}{c}, \quad (11)$$

Equations (10) are identical with the usual semiclassical equations for the slowly varying envelope fields [19, 20], except for the presence of the Langevin terms F that describe quantum fluctuations and depend on the bath and nonlinear atom-field coupling, and are expressed as:

$$\begin{aligned} F^\Omega(t, z) &= 2\xi^\alpha(t, z) \sqrt{G\kappa\bar{n}} = [F^{\Omega^\dagger}(t, z)]^*, \\ F^R(t, \mathbf{r}, \omega) &= \frac{1}{\sqrt{\rho(\mathbf{r}, \omega)}} \{ \xi^J(t, \mathbf{r}, \omega) \sqrt{u(\mathbf{r}_\perp) \Omega R^-} + 2\xi^P(t, \mathbf{r}, \omega) \sqrt{\gamma_P(R^3 + 1)} + 2\xi^o(t, \mathbf{r}, \omega) \sqrt{W_{12}} \}, \\ F^{R^\dagger}(t, \mathbf{r}, \omega) &= \frac{1}{\sqrt{\rho(\mathbf{r}, \omega)}} \{ \xi^{J^\dagger}(t, \mathbf{r}, \omega) \sqrt{u^*(\mathbf{r}_\perp) \Omega^\dagger R^+} + 2\xi^{P^*}(t, \mathbf{r}, \omega) \sqrt{\gamma_P(R^3 + 1)} + 2\xi^{o^*}(t, \mathbf{r}, \omega) \sqrt{W_{12}} \}, \\ F^z(t, \mathbf{r}, \omega) &= \frac{1}{\sqrt{\rho(\mathbf{r}, \omega)}} \{ \xi^z(t, \mathbf{r}, \omega) [2\gamma_\parallel (1 - \sigma^{SS} R^3) + (R^- u^*(\mathbf{r}_\perp) \Omega^\dagger + R^+ u(\mathbf{r}_\perp) \Omega) - 2W_{12} R^+ R^-]^{1/2} \\ &\quad - [\xi^o(t, \mathbf{r}, \omega) R^+ + \xi^{o^*}(t, \mathbf{r}, \omega) R^-] \sqrt{W_{12}} \}. \end{aligned} \quad (12)$$

The terms optical thermal noise $\xi^\alpha(t, z)$, incoherent pumping noise $\xi^o(t, \mathbf{r}, \omega)$ and collisional dephasing noise $\xi^P(t, \mathbf{r}, \omega)$ are complex, while photon-atom interaction noise $\xi^J(t, \mathbf{r}, \omega)$, $\xi^{J^\dagger}(t, \mathbf{r}, \omega)$ and $\xi^z(t, \mathbf{r}, \omega)$ are real. These noise terms are δ correlated. Since the equations are derived through a normally ordered representation, there are bath noise terms associated with dephasing (γ_P) and gain (W_{12}), but not losses (W_{12}). Furthermore, the gain noise is only present at finite temperatures. In addition to the bath noise, the positive- P method has noise associated with the atom-field coupling, which is present even for unitary evolution and corresponds in some sense to shot-noise effects in the atom-light interaction.

3. Simulation

We investigate theoretically the squeezing generated due to SIT solitons using mercury atoms, whose advantages have been already discussed in the Introduction. The atomic mercury contains seven isotopes with more than 5% abundance, including five bosonic and two fermionic isotopes that are stable. The fermions have low nuclear spin, simplifying the complexity of the hyperfine structure [21, 22]. Since bosonic and fermionic isotopes exhibit different dynamics, we will initially focus on the bosonic isotope ^{202}Hg , which has the highest abundance. The effect of other isotopes with their hyperfine structure will be included afterwards in the simulation.

In this case, we identify the $6^3\text{D}_3 \rightarrow 6^3\text{P}_2$ as the most suitable transition since it is associated with metastable states and can exhibit long coherence times (see Fig. 1). This is crucial for supporting long-lived soliton states.

We consider an optical hollow-core fiber that is ideally 50 mm long with a core diameter of $10 \mu\text{m}$ and filled with mercury vapor gas. We assume the atomic profile to be Lorentzian at zero temperature; however, at high temperatures, they have a Voigt profile. Experimentally, the fiber needs to be connected to a reservoir of Hg, from which one can change the density of atoms, thus the pressure through heating. This unavoidably yields a dead-volume which will be much larger than the volume of the fiber ($20 \mu\text{l}$ for a $10 \mu\text{m}$ diameter, 50 mm long fiber). The dead volumes will impose the pressure in the channel connecting the reservoir and the fiber.

We assume the gas is homogeneously distributed throughout the PCF, with the pressure being uniform along the entire fiber at the given temperature. The refractive index of two level atom [23] is approximately $\sqrt{1 + \chi}$:

$$\chi = N_j \frac{3\lambda_0^3 \gamma_0}{4\pi^2} \frac{i\gamma_0 - 2\delta}{\gamma_0^2 + 4\delta^2 + 2|\Omega|^2}, \quad (13)$$

where δ is the detuning and N_j is the number of atoms in each cell of the fiber. Since we are operating at low pressures, ranging from 10^{-8} to 10^{-7} bar (thus atomic density from 10^{11} to 10^{12}), the refractive index of the gas is approximately 1, and the gas dispersion can be considered negligible. Additionally, the waveguide has anomalous dispersion, which can vary depending on the geometry of the hollow core fiber. However, given that the fiber length is relatively short at 50 mm, we assume the dispersion to be negligible for the presented data.

Furthermore, in this regime, we neglect the effect of pressure broadening and incorporate its impact through the atom density.

To accurately account for the nonlinearity in each segment of the fiber where the atoms are located, we divide the fiber into multiple segments. When the gas is at a low temperature, the atomic transitions can be well-approximated by a delta function due to negligible thermal broadening. However, at room temperature, thermal effects cause the atomic transitions to broaden, resulting in a Voigt profile. In this paper, we will discuss both scenarios.

For convenience, we transform the Eqs. (10) into the retarded time frame, $\tau = t - z/v_g$, where the reference frame propagates with the pulse center along the z -direction at velocity v_g [16]. In this case, the pulse propagation follows:

$$\left[\frac{\partial}{\partial z} + \left(\frac{1}{c} - \frac{1}{v_g} \right) \frac{\partial}{\partial \tau} \right] \Omega(\tau, z) = -\frac{1}{2} \kappa \Omega(\tau, z) + \frac{G}{c} \int \rho(z, \omega) R^-(\tau, z, \omega) d\omega + F^\Omega(\tau, z).$$

and the atomic variables at each point along the fiber evolve in τ . We assume the atoms are initially distributed in the ground state, thus the polarization vectors R^\pm and the population inversion R^3 vectors are:

$$R^+ = R^- = 0, \quad R^3 = -1/2. \quad (14)$$

and the input coherent field, has the soliton shape

$$\Omega(0, t) = 2A \cosh^{-1}[A(\tau - \tau_0)] \exp\{i[\delta\tau + \phi(0)]\}, \quad (15)$$

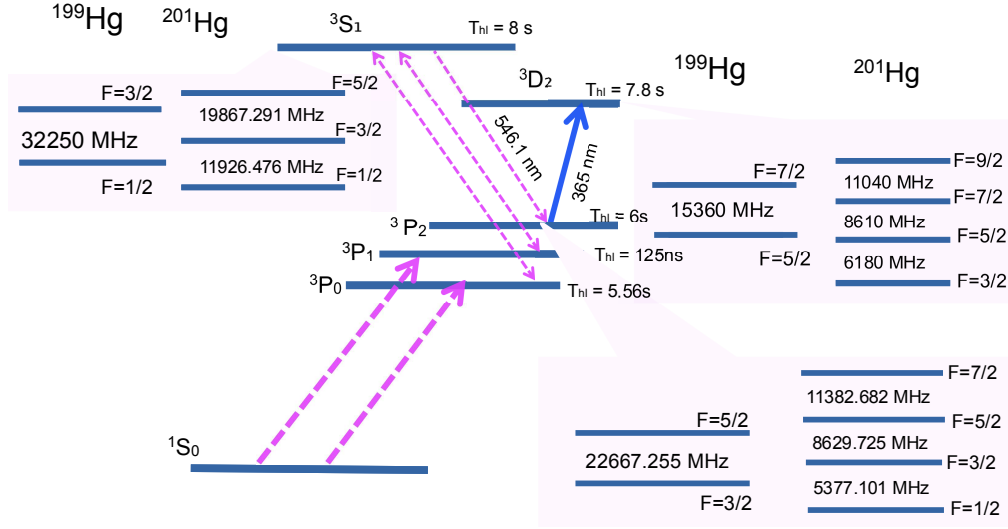


Fig. 1. The relevant energy levels for neutral mercury (hyperfine structure for the fermions is plotted). The suitable transition for the SIT is considered to be $6^3D_3 \rightarrow 6^3P_2$ transition.

where $2A$ is the pulse amplitude, τ the pulse timing in the retarded time frame, at $z = 0$, and δ is detuning of pulse.

The standard way of detecting squeezing is via homodyne detection with a local oscillator of amplitude f_{LO} that we take as normalized $\int |f_{\text{LO}}(t)|^2 dt = 1$. The normalized variances at the point z along the fiber is.

$$\hat{M}(z) = \int_{-\infty}^{\infty} \left\{ f_{\text{LO}}(t) \hat{\Omega}^\dagger(t, z) e^{i\theta} + f_{\text{LO}}^\dagger(t) \hat{\Omega}(t, z) e^{-i\theta} \right\} dt. \quad (16)$$

The corresponding squeezing ratio is

$$S(z) = \frac{\text{Var}[\hat{M}(z)]}{\text{Var}[\hat{M}]|_{\text{coh}}}, \quad (17)$$

where $\text{Var}[\hat{M}(z)] = \langle \hat{M}^2(z) \rangle - \langle \hat{M}(z) \rangle^2$.

To calculate the variance with a $+P$ simulation, we need to express it in terms of normally ordered correlations:

$$\hat{M}^2 \simeq : \hat{M}^2 : + \frac{4G}{v_g}, \quad (18)$$

where we have used the approximate equal-space commutation relation $[\hat{\Omega}(t, z), \hat{\Omega}^\dagger(t', z)] \simeq 4G\delta(t - t')/v_g$. The squeezing ratio is then

$$S = 1 + \frac{v_g \text{Var}_{+P}[\hat{M}]}{4G}, \quad (19)$$

where $\text{Var}_{+P} \equiv \langle : \hat{M}^2 : \rangle - \langle \hat{M} \rangle^2$.

4. Results

4.1. Low-temperature squeezing

We calculate the quadrature squeezing from the variances of Ω using Eq. 19 after the optical pulse starts propagating in the PCF. By adjusting the phase of the local oscillator f_{LO} , we can measure the squeezing at different phases at different propagation length.

The suitable transition for SIT is considered to be $^3D_2 \rightarrow ^3P_2$ with $\lambda_0 = 365.5$ nm. To fully excite this transition, we consider a pulse with a duration of $\frac{\tau c}{\lambda_0} = 0.44$, where $\tau = 4$ fs, and can excite the $^3S_1 \rightarrow ^3P_2$ transition that is accounted in the simulation.

We consider two scenarios. First, we focus on the bosonic isotope ^{202}Hg , as it has the highest abundance, then include the fermionic isotopes with their hyperfine structures shown in Fig 1. In the second scenario, we utilize each isotope abundance to determine its corresponding atomic density within the whole sample. Subsequently, we compute the polarization vectors R^\pm , R^3 for each given isotope separately. In the case of the bosonic isotopes, where $I = 0$, we only need to compute the Bloch vectors for the $6^3D_3 \rightarrow 6^3P_2$ and $^3S_1 \rightarrow ^3P_2$ transitions. However, for fermionic isotopes with $I \neq 0$, we must compute the Bloch vectors for each dipole-allowed transition in the hyperfine structure. Each of these transitions is computed separately and included in the nonlinear term. In this case, the nonlinear atom-field interaction term can be computed at a given position z where the atoms are located as follows:

$$\sum_{i=1} G_i \int R_i(z, \omega) \rho_i(z, \omega) d\omega \quad (20)$$

where G_i , ρ_i are the atomic-field interaction coefficient and the atomic density of i th isotope, respectively, and are given by $\rho_i(z, \omega) = A_i \rho_{\text{tot}}(z) f_i(\omega)$ where A_i is the abundance of isotope, ρ_{tot} is the total atomic density, $f_i(\omega)$ determines the lineshape of the atoms at the given temperature. R_i represents the polarization vector of i th isotope, which in the fermionic case, it is summed over the allowed transitions.

The atomic density is increased by raising the pressure through heating the gas. At $T = 273$ K, the gas pressure is taken to be 272×10^{-8} bar, which corresponds to an atomic number of approximately 14×10^{11} in the entire fiber, and have a Lorentzian lineshape.

Figure 2 (a) compares the optimum squeezing as a function of the detection phase of the local oscillator at 273 K. The maximum squeezing is achieved when a local oscillator phase is slightly away from zero ($\phi = -0.14$ rad). As the phase moves towards $\pi/2$ or $-\pi/2$, the optimal squeezing diminishes and eventually becomes zero. The optimum squeezing is calculated as the maximum squeezing over the entire fiber length.

Figure 2 (b) depicts the squeezing along the fiber at $\phi = -0.14$ rad. The fermionic isotopes ^{199}Hg and ^{201}Hg , encounter 30% of the mercury sample. The strength of the hyperfine transitions of these involved isotopes is in order of GHz. As it is clear from the Fig. 2, once these isotopes are considered in the simulation, the computed squeezing is slightly suppressed.

Figure 3(a) shows the optimum squeezing over the entire fiber length and the detection phases as a function of detuning (ranges from 0 to $16/\tau$). The black circle points show the optimum squeezing as a function of detuning. The red dashed line shows the squeezing at $\delta = 0$. Clearly, for a slightly detuned optical pulse ($\delta < 10^{-3}/\tau$), the squeezing exceeds its value compared to a pulse at resonance. Beyond this point, as the detuning increases, the squeezing gradually reduces to zero. This emphasizes that SIT squeezing at 273 K is achievable when the pulse and atoms are either at resonance or even slightly detuned.

Figure 3(b) shows the detection length L_{opt} of the optimal squeezing. By increasing the detuning, the detection length does not change with pulse on the resonance unless when the squeezing is diminished to zero.

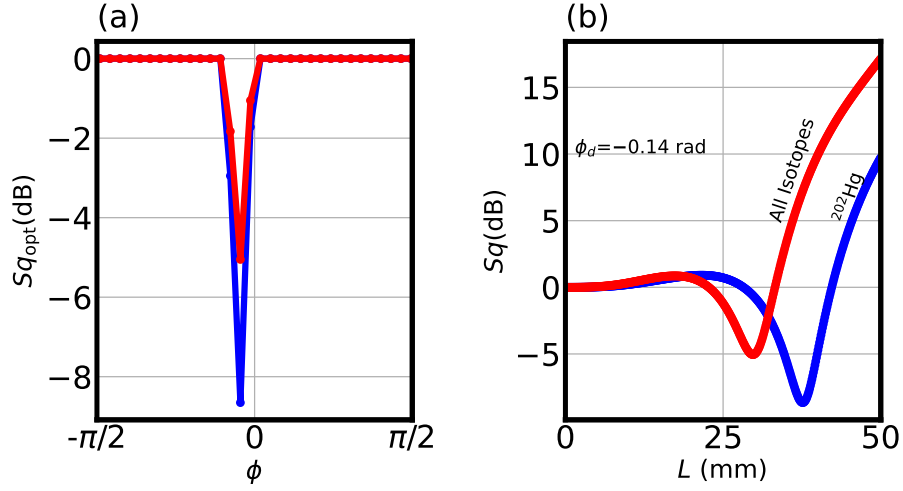


Fig. 2. (a) the optimum squeezing as a function of the local oscillator phase and (b) the squeezing at the optimum angle as a function of fiber length for the isotope ^{202}Hg (blue curve) and for a gas including all isotopes (red curve). The pulse duration is considered to be 4 fs, and the atom pressure corresponds to the vapor pressure of mercury at $T=273$ K.

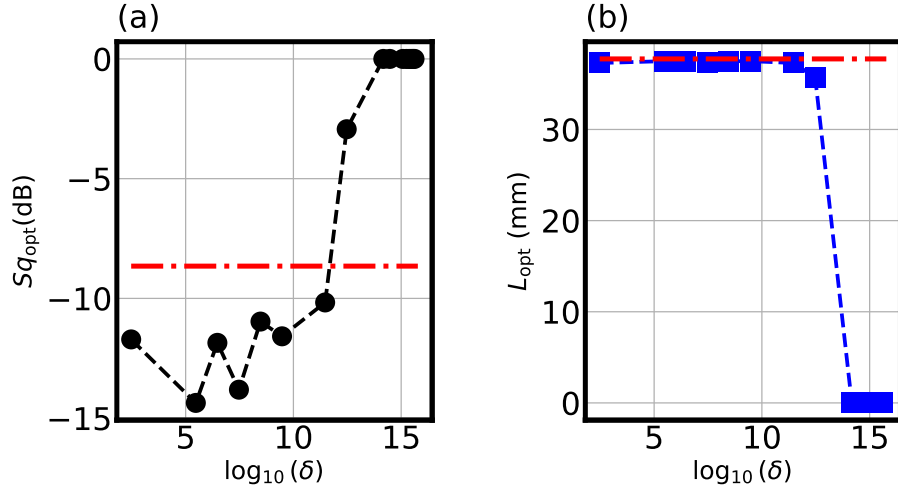


Fig. 3. (a) shows the optimum squeezing as a function of detuning, while (b) shows the detection length for the optimum squeezing as a function of detuning. The red dashed line indicates optimum squeezing at $\delta = 0$. The range of detuning changes from 0 to $16/\tau$. The pulse duration is $\tau = 4$ fs and atomic vapour pressure is $P = 272 \times 10^{-8}$ bar at $T = 273$ K.

4.2. Squeezing at room temperature

At the room temperature, atomic distribution forms a Voigt profile [24], $f_{\text{Voigt}}(\omega)$,

$$\sum_i G_i \int R_i(z, \Delta\omega_{\text{Voigt}}) A_i \rho_{\text{tot}}(z) f_{\text{Voigt}}(\omega) d\omega, \quad (21)$$

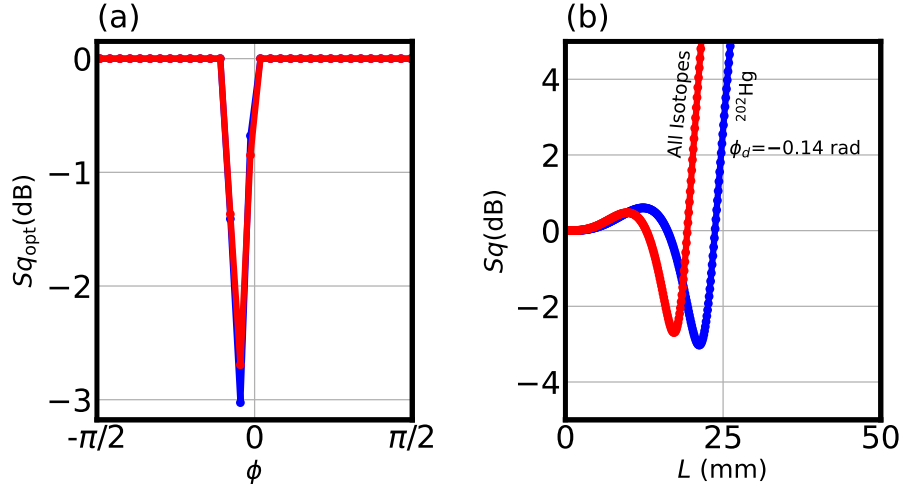


Fig. 4. The figure illustrates (a) the optimum squeezing as a function of the local oscillator phase and (b) the squeezing at the optimum angle as a function of fiber length for the isotope ^{202}Hg (blue curve) and for a gas including all isotopes (red curve). The pulse duration is considered to be 4 fs, and the atom pressure corresponds to the vapor pressure of mercury at $T = 293\text{K}$.

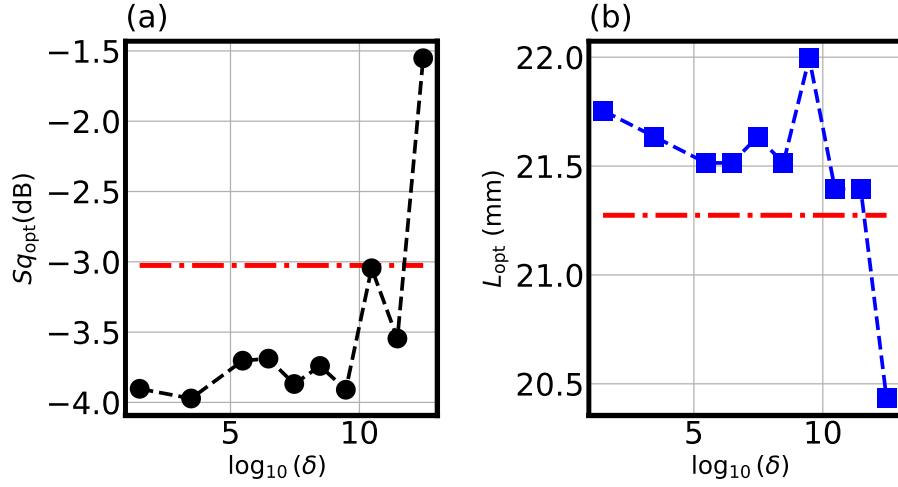


Fig. 5. (a) shows the optimum squeezing as a function of detuning, while (b) shows the detection length of the optimum squeezing. The red dashed line is the optimum squeezing at $\delta = 0$. The pulse duration is $\tau = 4\text{fs}$ and atomic vapour pressure is $P = 8.89 \times 10^{-6}$ bar at $T = 293\text{K}$.

where $\Delta\omega_{\text{Voigt}}$ is FWHM of the atomic Voigt profile and

$$\Delta\omega_{\text{Voigt}} = \frac{\Delta\omega_L}{2} + \sqrt{\Delta\omega_D^2 + 0.2166 \Delta\omega_L^2}, \quad (22)$$

where $\Delta\omega_L$ is the Lorentzian FWHM and

$$\Delta\omega_D^2 = \left(\frac{4\pi}{\lambda_0}\right) \sqrt{\frac{2 \log(2) k_b T}{m_i}} \quad (23)$$

is the Doppler FWHM at the temperature T . λ_0 is the wavelength of the selected transition, m_i is the isotope reduced atomic mass.

Figure 4 compares squeezing over the fiber length at 293 K using a coherent pulse on resonance with a duration $\tau = 4$ fs. For sufficiently short pulse duration, it is possible to achieve squeezing at room temperature, although the effect is not significant. Higher temperatures enhance damping and dephasing, leading to a reduction in squeezing.

As it is depicted in Fig. 5, the detuning leads to only 1dB enhancement of squeezing when the atomic absorption line shape follows a Voigt profile at a temperature of 293 K.

Figure 6 (a) compares the optimum squeezing as a function of pressure for isotope ^{202}Hg (blue circle point) with a sample including all isotopes (the red points). The optimum detection length Fig 6 (b) is also shown as a function of vapour pressure. As the pressure increases, the squeezing is suppressed, and the detection length becomes shorter. As can be seen, when all isotopes are included in the sample, the squeezing does not differ significantly from the case when only the isotope ^{202}Hg is considered.

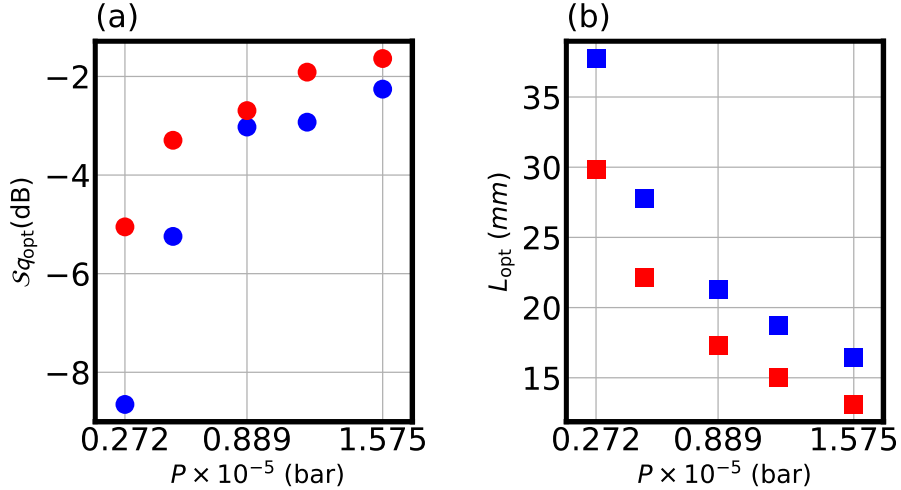


Fig. 6. (a) Optimum squeezing as a function of pressure, blue circle circles (only ^{202}Hg), the red circles, includes all isotopes. (b) the detection length for optimum squeezing as a function of pressure.

5. Concluding remarks

We have studied the feasibility of quantum squeezing using mercury vapor gas in a hollow-core photonic crystal fiber (PCF). Our findings show that the best squeezing is achievable at 273 K since damping suppresses squeezing. Mercury proves to be a promising candidate for SIT squeezing; however, careful consideration must be given to the selection of the pulse duration and wavelength. To fully excite this transition, we consider a pulse with a duration of $\tau = 4$ fs. The transition occurs at a wavelength of $\lambda = 365.5$ nm. To achieve this wavelength, it would typically require frequency conversion, such as third harmonic generation, from an Optical Parametric Oscillator (OPO) output. Furthermore, proper tuning of the pulse and optimization

of other parameters, such as gas pressure and fiber length, are crucial to maximize the squeezing effect.

Funding. Agencia Estatal de Investigación (PID2021-127781NB-100).

Acknowledgments. We acknowledge discussions with U. Vogl. and T. Dirmeier.

Disclosures. The authors declare no conflicts of interest.

Data availability. Data underlying the results presented in this paper are not publicly available at this time but may be obtained from the authors upon reasonable request.

References

1. S. L. McCall and E. L. Hahn, "Self-induced transparency by pulsed coherent light," *Phys. Rev. Lett* **18**, 908 (1967).
2. S. L. McCall and E. L. Hahn, "Self-induced transparency," *Phys. Rev.* **183**, 457 (1969).
3. G. L. Lamb, "Analytical descriptions of ultrashort optical pulse propagation in a resonant medium," *Rev. Mod. Phys.* **43**, 99–124 (1971).
4. R. E. Slusher, "Self-induced transparency," *Prog. Opt.* **12**, 53–100 (1974).
5. I. A. Poluéktov, Y. M. Popov, and V. S. Roitberg, "Self-induced transparency effect," *Sov. Phys. Usp.* **17**, 673 (1975).
6. A. I. Maimistov, A. M. Basharov, S. O. Elyutin, and Y. M. Sklyarov, "Present state of self-induced transparency theory," *Phys. Rep.* **191**, 1–108 (1990).
7. K. Watanabe, H. Nakano, A. Honold, and Y. Yamamoto, "Optical nonlinearities of excitonic self-induced-transparency solitons: Toward ultimate realization of squeezed states and quantum nondemolition measurement," *Phys. Rev. Lett.* **62**, 2257 (1989).
8. P. S. J. Russell, "Photonic-crystal fibers," *J. Light. Technol.* **24**, 4729–4749 (2006).
9. J. C. Travers, W. Chang, J. Nold, *et al.*, "Ultrafast nonlinear optics in gas-filled hollow-core photonic crystal fibers," *J. Opt. Soc. Am. B* **28**, A11–A26 (2011).
10. P. Ghenuche, S. Rammler, N. Y. Joly, *et al.*, "Kagome hollow-core photonic crystal fiber probe for Raman spectroscopy," *Opt. Lett.* **37**, 4371–4373 (2012).
11. R. Yu, Y. Chen, L. Shui, and L. Xiao, "Hollow-core photonic crystal fiber gas sensing," *Sensors* **20**, 2996 (2020).
12. D. R. Häupl, D. Weller, R. Löw, and N. Y. Joly, "Spatially resolved spectroscopy of alkali metal vapour diffusing inside hollow-core photonic crystal fibres," *New J. Phys.* **24**, 113017 (2022).
13. U. Vogl, C. Peuntinger, N. Y. Joly, *et al.*, "Atomic mercury vapor inside a hollow-core photonic crystal fiber," *Opt. express* **22**, 29375–29381 (2014).
14. P. Drummond and M. Raymer, "Quantum theory of propagation of nonclassical radiation in a near-resonant medium," *Phys. Rev. A* **44**, 2072 (1991).
15. P. D. Drummond and C. W. Gardiner, "Generalised p -representations in quantum optics," *J. Phys. A: Math. Gen.* **13**, 2353 (1980).
16. M. Najafabadi, L. Sánchez-Soto, J. Corney, *et al.*, "Quantum squeezing via self-induced transparency in a photonic crystal fiber," *Phys. Rev. Res.* **6**, 023142 (2024).
17. C. W. Gardiner and P. Zoller, *Quantum Noise* (Springer, Berlin, 2004), 2nd ed.
18. A. Gilchrist, C. W. Gardiner, and P. D. Drummond, "Positive p representation: Application and validity," *Phys. Rev. A* **55**, 3014–3032 (1997).
19. M. Lax, "Quantum noise. iv. quantum theory of noise sources," *Phys. Rev.* **145**, 110–129 (1966).
20. H. Haken and W. Weidlich, "Quantum noise operators for the n -level system," *Zeit. Phys.* **189**, 1–9 (1966).
21. S. Mejri, J. J. McFerran, L. Yi, *et al.*, "Ultraviolet laser spectroscopy of neutral mercury in a one-dimensional optical lattice," *Phys. Rev. A* **84**, 032507 (2011).
22. P. Villwock, S. Siol, and T. Walther, "Magneto-optical trapping of neutral mercury," *The Eur. Phys. J. D* **65**, 251–255 (2011).
23. R. A. McCutcheon and S. F. Yelin, "Limits and possibilities of refractive index in atomic systems," *Opt. Commun.* **505**, 127583 (2022).
24. T. T. García, "Voigt profile fitting to quasar absorption lines: an analytic approximation to the voigt–hjerting function," *Mon. Notices Royal Astron. Soc.* **369**, 2025–2035 (2006).